Journal of Applied Physics ARTICLE scitation.org/journal/jap

Interplay of intrinsic and extrinsic states in pinning and passivation of *m*-plane facets of GaN *n*-*p*-*n* junctions

Cite as: J. Appl. Phys. **128**, 185701 (2020); doi: 10.1063/5.0020652
Submitted: 2 July 2020 · Accepted: 19 October 2020 ·
Published Online: 9 November 2020

L. Freter,[1,2,a)] Y. Wang,[1,2] M. Schnedler,[1] J.-F. Carlin,[3] R. Butté,[3] N. Grandjean,[3] H. Eisele,[4] R. E. Dunin-Borkowski,[1,5] and Ph. Ebert[1,b)]

AFFILIATIONS

[1]Peter Grünberg Institut, Forschungszentrum Jülich GmbH, 52425 Jülich, Germany
[2]Lehrstuhl für Experimentalphysik IV E, RWTH Aachen University, 52056 Aachen, Germany
[3]Institute of Physics, Ecole Polytechnique Fédérale de Lausanne (EPFL), 1015 Lausanne, Switzerland
[4]Technische Universität Berlin, Institut für Festkörperphysik, Hardenbergstr. 36, 10623 Berlin, Germany
[5]Ernst Ruska-Centrum, Forschungszentrum Jülich GmbH, 52425 Jülich, Germany

[a)]**Email:** l.freter@fz-juelich.de
[b)]**Author to whom correspondence should be addressed:** p.ebert@fz-juelich.de

ABSTRACT

Intrinsic and extrinsic pinning and passivation of *m*-plane cleavage facets of GaN *n*-*p*-*n* junctions were investigated by cross-sectional scanning tunneling microscopy and spectroscopy. On freshly cleaved and clean *p*-type GaN($10\bar{1}0$) surfaces, the Fermi level is found to be extrinsically pinned by defect states, whereas *n*-type surfaces are intrinsically pinned by the empty surface state. For both types of doping, air exposure reduces the density of pinning states and shifts the pinning levels toward the band edges. These effects are assigned to water adsorption and dissociation, passivating intrinsic and extrinsic gap states. The revealed delicate interplay of intrinsic and extrinsic surface states at GaN($10\bar{1}0$) surfaces is a critical factor for realizing flatband conditions at sidewall facets of nanowires exhibiting complex doping structures.

I. INTRODUCTION

Group III-nitride (III-N) semiconductors evolved into the materials of choice for blue and UV opto-electronics as well as high-power electronics[1–4] and are also becoming increasingly attractive for bio-electric devices based on surface functionalizations.[5] These applications are primarily based on planar heterostructures. However, III-N semiconductor nanowires offer new degrees of strain management, allowing for the extension of opto-electronics over the whole visible range.[6–8] Furthermore, such nanowires can be used in solar cells to make the charge carrier separation direction independent of the illumination and hence absorption direction. The large surface to volume ratio is also highly attractive for enhancing the sensitivity of bio-electric devices.

However, the nanowires' large surface fraction causes recombination and Fermi level pinning at surfaces to be a highly critical factor. Therefore, electronic passivation of nanowire facets is of high importance for successful applications. The dominant facets of III-N nanowires are the non-polar *m*-plane sidewall surfaces. For *n*-doped *m*-plane GaN, it has recently been demonstrated that the empty intrinsic Ga-derived dangling bond surface state creates an upward band bending, separating holes and electrons, and hence reducing recombination.[9,10] Unfortunately, this cannot suppress recombination at *p*-*n* junctions. *p*-type GaN is, however, a prerequisite for the functioning of opto-electronic, solar cell, and bio-electric sensing devices. For general suppression of recombination a real passivation, i.e., reduction of the density of surface recombination centers is needed.

Therefore, we investigated the electronic structure of the *m*-plane cross-sectional cleavage surface of a *n*-*p*-*n* GaN junction using scanning tunneling microscopy (STM) and spectroscopy

(STS). We identify the pinning levels of the Fermi energy and their physical origin for clean and air-exposed surfaces. For *p*-type GaN *m*-plane surfaces, we identify extrinsic states at cleavage steps as the origin of the Fermi level pinning, in contrast to the intrinsic empty Ga-derived dangling bond being relevant for *n*-type GaN($10\bar{1}0$) surfaces. Air exposure induces a passivation of the extrinsic and intrinsic surface states, primarily by water adsorption and dissociation. This passivation, i.e., a shift of the pinning levels toward the band edges, enables the growth of unpinned GaN nanowire *n-p-n* junctions (or more complex doping structures) for device applications.

II. EXPERIMENT

The *n-p-n* GaN epilayer structure was grown by metalorganic chemical vapor deposition (MOCVD) on a free-standing *n*-type GaN pseudosubstrate at 960 °C. For the *n*-type and *p*-type doping, Si and Mg dopants were incorporated, respectively. The average dopant concentrations were [Si] 3×10^{18} cm^{-3}, [Mg] 1×10^{19} cm^{-3}, and [Si] 9×10^{18} cm^{-3} within the *n-p-n* GaN structure, respectively. The Mg dopants were thermally activated at 650 °C. Then, the sample was overgrown by an n^{++}-type capping layer at 715 °C.

Samples cut from the wafer were cleaved *in situ* in ultrahigh vacuum (UHV) ($p < 2 \times 10^{-8}$ Pa) and directly investigated *in situ* by cross-sectional STM using tungsten tips. Afterward, the samples were transferred through air in order to be investigated by scanning electron microscopy (SEM). The such investigated samples were then reinserted into the STM in UHV. For this, the samples were heated in the load lock at approximately 110 °C for 4 days. In addition, secondary ion mass spectroscopy was applied to quantify the dopant concentrations.

During STM measurements, grids of current–voltage tunneling spectra were acquired to achieve a so-called current imaging tunneling spectroscopy (CITS) mapping.

III. RESULTS

Figures 1(a)–1(c) illustrate an overview of the *n-p-n* GaN structure acquired with three different imaging methods. The different layers can be discerned well in the SEM image (a). On the far left side, one can see the substrate, which is separated from the first *n*-doped layer by a bright thin interface. This interface is due to a delta-type Si-doped layer approximately 20 nm wide.[11] The following *n-p-n* structure consist of perfect epitaxial layers. Only the capping layer on the far right turned to 3D growth due to the low growth temperature. For the STM/STS experiments, we focused on the *n-p-n* layers only.

The constant-current STM image [Fig. 1(c)] exhibits multiple cleavage steps with smaller contrast, primarily oriented along the *c*[0001] direction. In addition, a strong contrast change is found at both *n-p* and *p-n* interfaces. Since the tunnel current is sensitive to height changes but also to materials' electronic properties, the contrast between *p*- and *n*-doped layers is a combination of topographic (cleavage step along the *a* direction) and electronic effects. In order to unravel the origin of the contrast at the *n-p* junctions, we acquired a CITS map at −3.2 V [Fig. 1(b)]. The CITS map indicates a strong electronic contrast between the *n*- and *p*-doped regions.

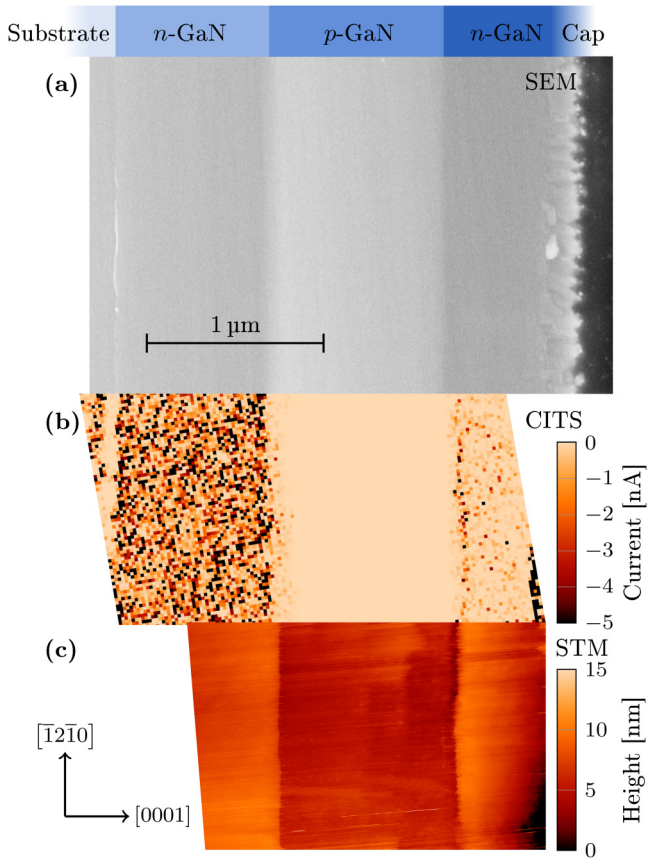

FIG. 1. Cross-sectional overview of the *n-p-n* GaN structure. (a) SEM image in the secondary electron mode (5 keV), (b) CITS map at −3.2 V (tip–sample distance fixed at +6 V and 80 pA), and (c) constant-current STM image acquired at −2.5 V and 80 pA. The doping junctions can be discerned well by each method. The CITS map and the STM image were acquired after reinsertion and annealing in UHV (see Sec. II).

A. Tunneling spectroscopy on clean cleavage surfaces in UHV

To visualize this electronic contrast, a spatial evolution of tunneling spectra across the clean, freshly cleaved *n-p-n* structure in UHV is shown in Fig. 2(a). At the *n*-doped layer (blue spectra), the negative and positive branches of the *I–V* curves have a similar shape just mirrored. In contrast, at the *p*-doped layer (red spectra), the positive branch reaches much higher absolute currents at the same absolute voltages. The spatial dependence of this asymmetric behavior can be illustrated by calculating the average current for a symmetric voltage range across the *n-p-n* structure. The resulting spatial dependence of the average current as asymmetry indication is shown in Fig. 2(b) for a voltage range of −2.3 V to +2.3 V. The blue spectra in the *n*-doped region have a near 0 average current (blue circles in Fig. 2), in agreement with the symmetric positive and negative current branches. The spectra probed in the *p*-doped region have

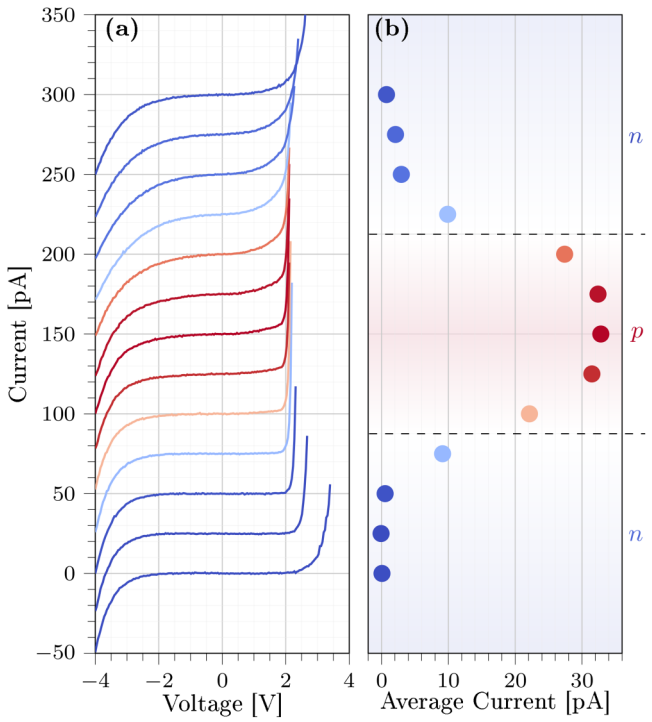

FIG. 2. (a) Spatial evolution of current–voltage spectra across the *n*-*p*-*n*-layers (setpoint −4 V and 50 pA) acquired on freshly cleaved, clean GaN surfaces in ultrahigh vacuum. Every spectrum displayed is the median of 490 single tunneling spectra measured in a rectangular spatial area two pixels wide in the *c* direction (corresponding roughly to 23 nm). The equidistant spatial separation between consecutive rectangular surface areas is approximately 70 nm in the *c* direction (hence, also the spatial separation between consecutively shown median spectra). For better visibility, consecutive spectra are offset by 25 pA. The current is cut off at approximately 50 pA for display purposes only. (b) Averaged current in the voltage range from −2.3 V to +2.3 V for the spectra shown in (a). Red spectra exhibit an asymmetric behavior, i.e., the average current is much larger than zero (red circles). This points to *p*-type material characteristics. Blue spectra are rather symmetric, consistent with *n*-type material characteristics.

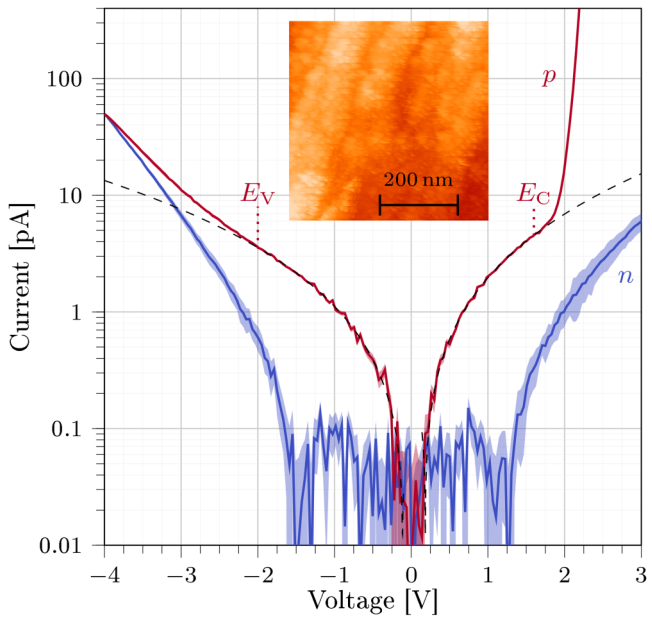

FIG. 3. Current–voltage (*I*–*V*) spectra obtained at the centers of the *p*- and *n*-doped layers exposed on freshly cleaved, clean GaN surfaces in ultrahigh vacuum. The *n*- (blue line) and *p*-type (red line) spectra are the medians of 10230 and 7225 single spectra, respectively. The background shadows indicate the respective error margins. The data are extracted from the same measurement as that in Fig. 2. The tip–sample separation was fixed at −4 V and 50 pA. The dashed curve is a fit to the first current onsets of the spectrum measured on the *p*-doped layer. The constant-current STM image (setpoint +6 V and 80 pA) of the *p*-doped layer in the inset demonstrates the high step density inducing a Fermi level pinning.

a high current asymmetry showing up as large average currents (red circles in Fig. 2).

Next, we analyze the tunneling spectra in more detail. For this, we turn to the logarithmic representation of the spectra shown in Fig. 3. First, we address the *n*-type spectrum acquired in the center of the first *n*-type layer (the blue line in Fig. 3). The spectrum exhibits a similar behavior than those measured previously on *n*-type GaN cleavage surfaces.[9,12] This behavior is determined by (i) an apparent bandgap smaller than the actual one and (ii) an upward shift of the conduction band current onset to higher positive voltages as compared to that expected for unpinned *n*-type semiconductors. This has been attributed to the presence of the empty Ga-derived dangling bond surface state within the bandgap,[9,13–15] which pins the Fermi level. The pinning induces the upward shift of the conduction band tunnel current onset to about +1 V.[12] Note that the empty Ga-derived dangling bond surface state has a strong dispersion. In the case of an empty surface state, a Fermi level pinning requires a partial filling of this state. This filling is only taking place at the minimum of the band dispersion. Hence, the pinning level is given by the minimum of the Ga-derived dangling bond surface state $S_{\mathrm{Ga,min}}$, and, thus, we probe the lowermost tail of the local density of states of the surface state but not the maximum. In contrast, at negative voltages, the current is originating from the tip-induced electron accumulation zone in the conduction band but not from tunneling out of valence band states. As a result, the fundamental bandgap is not probed.[16]

The spectrum measured in the center of the *p*-type layer (red line) exhibits a fundamentally different behavior: first, the apparent bandgap is extremely small. Second, at positive voltages, a second strong current onset is observed at about +1.6 V. Similarly, a weaker second onset occurs at negative voltages at about −2 V. These onsets were determined on the basis of the curvature reversal. The second onsets can be furthermore visualized by fitting the first current onsets with the voltage V dependence of the tunnel current I, which is governed by the exponential transmission coefficient. Based on Eq. 24 in Ref. 17, the voltage dependence of the tunnel current is given in the first approximation by $I \sim \exp(\alpha \times |V - V_{\mathrm{onset}}|^{0.5})$ with α being a constant and V_{onset} taking into account the shift of

the surface band edges relative to E_F.[17,18] The best fits, found for an exponent of about 0.25, are shown as dashed lines in Fig. 3.

The spectrum's shape can be understood as follows: the very small apparent bandgap suggests the presence of surface states pinning the Fermi energy near the midgap position. Visibly, electrons can tunnel into and out of these surface states, which indicate that the surface states are half filled. The fact that the current out of the surface states is lower than the current onset at higher voltages suggests that the density of states (DOS) of the midgap states is significantly lower than that of the states contributing to the second current onsets at higher magnitudes of voltage. This indicates that the surface states pinning the Fermi energy are related to defects, whereas the second onsets are arising from tunneling into the conduction and valence bands. This is corroborated by the voltage separation of the second onsets (−2 V and +1.6 V), which agrees very well with the fundamental bandgap of GaN at room temperature of approximately 3.4 eV.

At this stage, we address the pinning states. As outlined above, they can be attributed to defect states only since intrinsic surface states on GaN(10$\bar{1}$0) are first of all not in midgap position: the empty surface state is less than 1 eV below the conduction band, whereas the filled surface state is very close to the valence band edge. Second, the DOS of intrinsic surface states would be much larger and comparable to the DOS of the band edges. The constant-current STM image and the SEM image both suggest that the surface morphology is dominated by a large density of cleavage steps. The large cleavage step density can be attributed to the presence of strain within the epitaxial GaN structure in analogy to other strained systems investigated previously, i.e., strained Te-doped GaAs or quantum dots, where steps appear predominantly in the strained regions.[19–21] Indeed, it has been shown that high Si doping concentrations lead to lattice constant changes in GaN,[22] ultimately giving rise to strain in GaN epitaxial layers with doping profiles. We anticipate that this creates many different cleavage starting points and suppresses a smooth passage of the crack front through the remaining epitaxial structure during the cleavage process. The resulting surface steps and step kinks are known to exhibit localized states, which are typically half filled and in midgap position. Hence, we attribute the pinning on the *p*-type material to such cleavage steps. Note, the intrinsic filled N-derived dangling bond state and the nitrogen bulk vacancy's charge transfer level are too close to the valence band edge[9,23–26] and hence cannot be responsible for the pinning on *p*-type surfaces at midgap energies.

For *n*-type GaN(10$\bar{1}$0) surfaces, the effect of steps is less pronounced since the density of intrinsic empty surface states is larger than that of the steps and the intrinsic surface state is energetically above the step-induced states. Therefore, the Fermi level will be pinned first by the empty surface state. In contrast, for *p*-type GaN, the situation is different. First, the filled intrinsic N-derived surface state is at/close to the valence band edge. Second, the activation of the Mg dopants is always rather small, and hence the Fermi level is typically relatively far above the valence band maximum. Therefore, the filled intrinsic N-derived surface state cannot act as a pinning level (as it is fully filled), and the first available pinning level arises from the cleavage steps.

Finally, if the *p*-type GaN(10$\bar{1}$0) surface was unpinned, the spectra would also be fundamentally different from those measured on *n*-doped GaN(10$\bar{1}$0) surfaces. For unpinned *p*-type surfaces, no electrons would be in the conduction band under (non-equilibrium) tunneling conditions, even if the conduction band edge is dragged below the Fermi energy by the tip's electric field. Hence, no tunneling current of electrons from the conduction band into the tip can occur at negative voltages.[27] Thus, on *p*-type surfaces, no electron accumulation current occurs at negative voltages. The analogous hole accumulation current of electrons tunneling from the tip into the hole accumulation zone in the valence band at positive voltages can be neglected: the barrier for tunneling directly into the conduction band is much smaller (due to the large bandgap), and hence the normal conduction band current dominates. Hence, even for unpinned *p*-type material, the fundamental bandgap is detectable in contrast to *n*-type material.[16] This corroborated the assignment of the differently doped layers in our structure.

B. Tunneling spectroscopy on surfaces after exposure to ambient conditions

The CITS map and tunneling spectra in Figs. 1 and 4, respectively, indicate that after air exposure and reinsertion into UHV with annealing, the differently doped layers of the *n*-*p*-*n* GaN structure

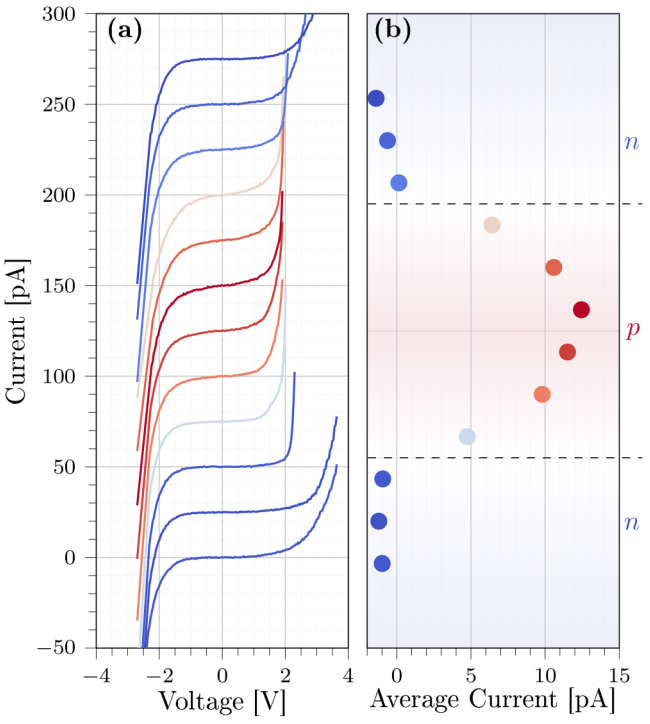

FIG. 4. (a) Spatial evolution of tunneling spectra across the *n*-*p*-*n*-layers after air exposure, evaluated in analogy to Fig. 2 (setpoint -2.5V and 80 pA). Each spectrum is the median of at least 460 single spectra. The spatial distance between two consecutive spectra is roughly 90 nm. (b) Average current (from −2.1 V to +2.1 V) of the spectra shown in (a). Spectra (red) at the *p*-doped layer exhibit a positive asymmetric behavior (the average current is strongly positive), whereas spectra (blue) at the *n*-doped layer have a small negative average current.

can be well recognized. The spectra exhibit again an asymmetry change across the *n*-*p* and *p*-*n* junctions (Fig. 4). This shows up, in particular, as a strong current change for the positive current branch [Fig. 4(a)], which leads to a significant increase in the asymmetry on the *p*-doped layer [Fig. 4(b)]. In addition, a reversal of the asymmetry occurs between *n*- and *p*-doped areas, in agreement with tunneling spectra obtained on GaAs(110) *n*- and *p*-junctions.[27–29]

At this stage, we turn to the detailed analysis of the spectra in Figs. 5 and 6. The general shape of the tunneling spectrum at the *p*-doped GaN(10$\bar{1}$0) surface after exposure to air and reintroduction into UHV with long term annealing is similar to that measured on freshly cleaved clean surfaces. At positive voltages, two current onsets can be observed, one around +0.8 V and the second one around +2 V. Similar, but somewhat less pronounced, two current onsets are present at negative voltages (−0.8 V and −1.5 V). The presence of two onsets is again corroborated by fitting the first onsets with the transmission coefficient based voltage dependence of the current (see above). The best fits obtained for an exponent of about 0.5 are shown as dashed lines. The voltage difference between the second current onsets (at positive and negative voltages) of 3.5 V corresponds again well to the fundamental bandgap of 3.4 V, considering thermal broadening as well as minor remaining tip-induced band bendings.

Despite all similarities, there are nevertheless some differences: These concern primarily the apparent bandgap being larger and the pinning position being shifted toward the valence band by a few tenth eV as compared to the freshly cleaved clean surface.

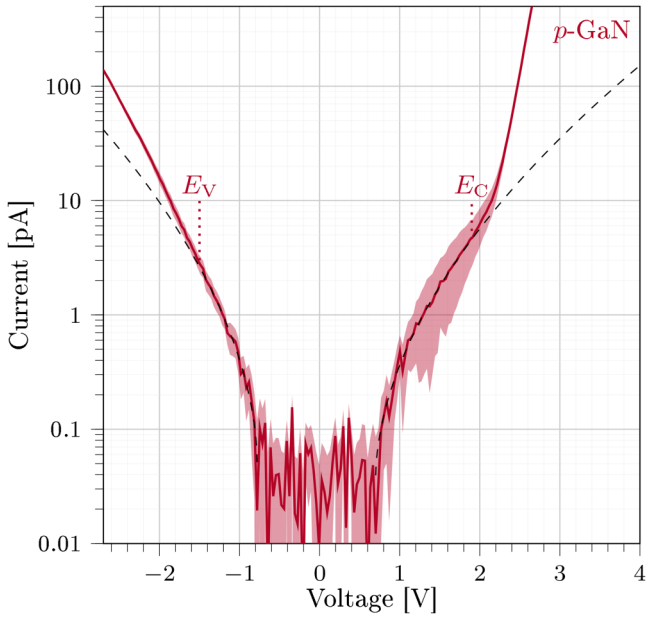

FIG. 5. Characteristic *I*–*V*-spectra obtained at the *p*-doped layer after air exposure. The setpoint is at −2.5 V and 80 pA. The dashed curve is a fit to the first current onsets of the spectrum measured at the *p*-doped layer. The background shadow indicates the error margin.

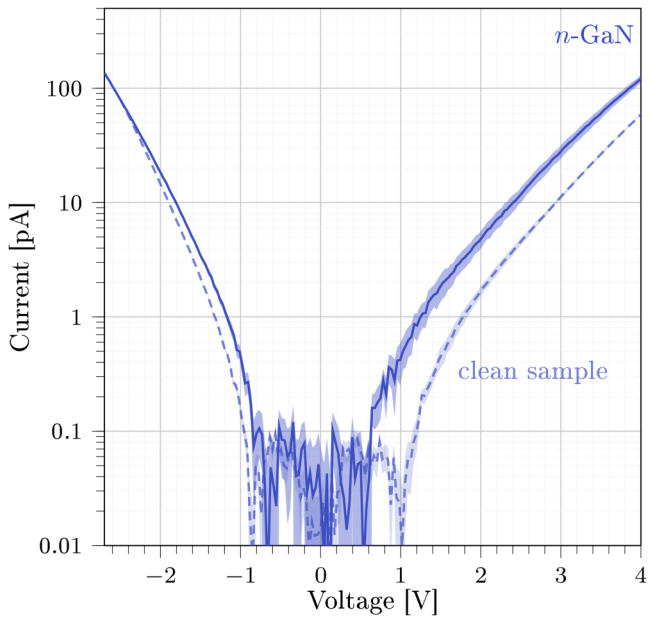

FIG. 6. Characteristic *I*–*V*-spectra obtained at the *n*-doped layer after air exposure (solid blue line). The setpoint is at −2.5 V and 80 pA. For comparison, a spectrum at the same setpoint from the *n*-type substrate of the clean sample is also displayed as a dashed blue line. The background shadow indicates the error margin.

The tunnel spectrum acquired at the *n*-doped layer after air exposure (blue line) exhibits very similar characteristics as those probed with identical set voltage and set current on a freshly cleaved *n*-type GaN surface (the dashed line). Only the current onset at positive voltages is shifted downward to approximately +0.5 V (Fig. 5). Note that we observed also a similar shift for tunneling spectra measured on the *n*-type GaN free-standing substrate's (10$\bar{1}$0) cleavage surface after air exposure and reinsertion into UHV.

IV. DISCUSSION OF EFFECT OF AIR EXPOSURE

At this stage, we address the origin of the electronic changes due to air exposure. First of all, the almost unchanged doping sensitivity of the spectra (i.e., asymmetry of *I*–*V* spectra at *p*- and *n*-doped layers) after air exposure is indicative of rather clean surfaces without significant oxidation due to air exposure and reinsertion into UHV with heating. Nevertheless, the spectra reveal some changes, which are: (i) the pinning DOS is reduced at the *p*-type surface and the pinning level is shifted slightly downward and (ii) similarly, the pinning level of the empty surface state is shifted upward at the *n*-doped surface.

We anticipate that both phenomena are induced by air exposure, which primarily leads to adsorption of oxygen and water molecules on the cleaved GaN(10$\bar{1}$0) surfaces. Other gases have a negligible concentration or are not reactive (nitrogen) and, thus, can be discarded in the discussion. For many semiconductors, such as, e.g., GaAs and Si, oxidation is the dominant process reaching deep into the bulk, when these materials are subjected to ambient

conditions at room temperature. In contrast, GaN behaves differently: no detectable oxidation of GaN has been observed for temperatures below 700 °C.[30,31] In addition, the sticking coefficient of oxygen on GaN(10$\bar{1}$0) surfaces is much lower than that of water.[32] Indeed, recent reports rather indicate that the adsorption and subsequent dissociation of water molecules is the preferred reaction process on polar GaN surfaces.[33,34]

On the non-polar GaN(10$\bar{1}$0) surface, the adsorption and following dissociation of water molecules occurs too: the dissociation barrier is found in theoretical calculations and experiments to be extremely small, i.e., in the low meV range.[35–37] Hence, this implies that the surface will be covered almost instantly by dissociated water, i.e., much faster than any oxidation can take place. In the final hydroxylation state, the OH^- group and the H^+ ion are bound to the Ga and N surface atoms, respectively.[34–36,38] This configuration is the most stable with a rather high dissociation energy of 1.44 eV.[35] The Ga–O–H bonds can be broken up only above 200 °C.[32,37] This indicates that the annealing of our air-exposed sample to 110 °C during baking in the load lock of the UHV chamber was insufficient to remove the layer of dissociated water molecules from the GaN *m*-plane surface.

Electronically, the bonding of the dissociated water at the surface atoms shifts both the N and Ga-derived dangling bonds toward the valence band edge, emptying the fundamental bandgap of intrinsic surface states (see Fig. 7): the N–H bond is energetically positioned below the valence band edge[39] and the Ga–OH bond is found at the valence band edge.[36,38]

Indeed, the assumption of H_2O-driven passivation of differently doped GaN layers agrees well with our STS measurements.

***p*-type GaN:** As reported above, we observed a very high step density on the *m*-plane cleavage surfaces by STM. Step edges and kinks correspond to either *a*- or *c*-plane facets with the latter being dominant on the investigated sample. These step edges and kinks induce defect states that are responsible for a Fermi level pinning of the clean, freshly cleaved *p*-type GaN(10$\bar{1}$0) surface measured by STS.

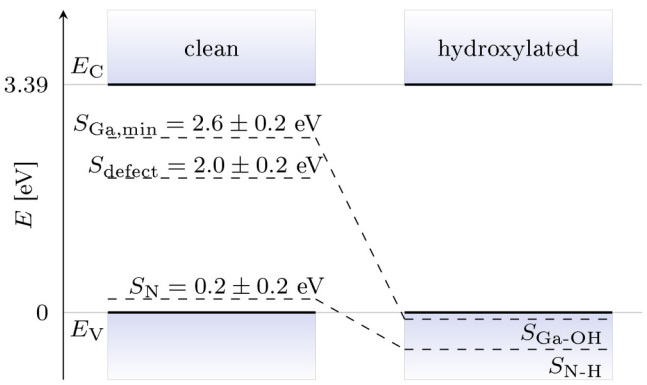

FIG. 7. Schematic band diagram showing the energy levels of the different states (intrinsic surface states, defect states, and hydroxilated intrinsic surface states) for the clean and hydroxilated *m*-plane GaN surface. The energy levels were extracted from our measurements (S_{defect} and $S_{Ga,min}$) and Refs. 36 and 39.

One can anticipate that hydroxylation will also modify these step edges and kinks: steps with *a*-plane facets can be expected to behave as *m*-plane surfaces, i.e., the hydroxylation (or hydrogen adsorption) will shift the intrinsic surface states into the valence band. Similarly, the intrinsic surface states of N- and Ga-terminated *c*-plane facets were found to shift into the valence band upon hydroxylation[33,40,41] or hydrogen adsorption.[42] Hence, one can expect that hydroxylation passivates step edges. This is in agreement with the experimental observations made for the *p*-type GaN(10$\bar{1}$0) surface, i.e., a reduced density of defect states and a shift of the pinning levels. The fact that the pinning level has been shifted but not removed completely indicates that step edges are only partially hydrated in agreement with the above expectation.

Furthermore, if the steps would be fully passivated and, thus, no step states remain within the fundamental bandgap, then we would not observe any tunneling features related to cleavage steps, anymore. Since this is not completely the case, we conclude that step states are partially passivated.

We anticipate that exposure to pure water (not air) could ultimately lead to a full passivation.

***n*-type GaN:** For clean *n*-type GaN(10$\bar{1}$0) surfaces, the minimum of the Ga-derived empty dangling bond state defines the surface Fermi level pinning as outlined above. This pinning induces an upward band bending of roughly 1 eV for the clean surface. For the air-exposed surface, the upward band bending is reduced to about 0.5 eV. The reduction of the band bending upon air exposure is corroborated by electroreflectance measurements.[43]

The reduced upward band bending can be explained with the passivation of the empty Ga-derived dangling bonds by OH^- groups shifting the resulting filled Ga–OH state to the valence band edge.[36,38] This hydroxylation can be anticipated to passivate most but not all Ga dangling bonds. As a result, the density of pinning states is reduced, driving the band bending back toward flatband conditions. This is consistent with the observation of a reduced upward band bending. If the surface would be fully passivated, then the onset of the current at positive voltages would be at 0 V. The fact that the onset voltage approaches, but not reaches 0 V, is indicative of a partial passivation. Again, we anticipate that exposure to pure water could lead to a full passivation.

It is noteworthy that, in our case, we cannot detect any indication that the OH^- bonding to the Ga dangling bond surface state is different for *n*- and *p*-type doping. Hence, there is, thus, far no indication of the Fermi level dependent selective surface reactions.

Finally, we discuss hydroxylation and adsorption on other GaN surface orientations and other molecule adsorption on *m*-plane GaN surfaces. On the one hand, hydroxylation has been investigated on *c*-plane GaN surfaces, too. On the *c*-plane surface, the adsorption of hydroxyl groups is preferred near the H3 site but not at the Ga location (the T4 site).[44] Hence, the binding structure is not comparable with that on the *m*-plane surface. Interestingly, at high hydroxyl concentrations, the pinning of the Ga surface state of the *c*-plane surface is lifted.[45] This tendency agrees with that observed here on the *m*-plane GaN surface. On the other hand, the binding of other types of molecules was investigated on *m*-plane GaN surfaces. It is found that the sulfur atom of thiol groups is bound to the Ga dangling bond,[46] in analogy to the adsorption of the OH^- group. This suggests that the complex negatively charged molecule groups

generally bind to the empty Ga dangling bond. This site is likely preferred due to the cation character of Ga in GaN.

For completeness, we provide at this stage, a critical reflection about the conclusions and methodology used. Besides, the here presented interpretation one could imagine that other effects, such as pure hydrogen passivation or oxygen coverage, could result in similar tunneling spectra. However, when taking into account, the literature results on adsorption of different molecules on GaN, the most plausible interpretation is the one outlined above. In addition, the energy levels of clean and hydroxylated surface states derived from the literature agree with the observations.

V. CONCLUSION

GaN *n-p-n* junctions were investigated by cross-sectional scanning tunneling microscopy and spectroscopy. Freshly cleaved clean cross-sectional surfaces in ultrahigh vacuum were compared with surfaces subjected to air exposure. At a freshly cleaved and clean *n*-type GaN($10\bar{1}0$) surface, the Fermi level is found to be intrinsically pinned by the empty Ga-derived surface state, whereas for *p*-type material, it is extrinsically pinned by defect states. Air exposure followed by heating in UHV reduces the density of pinning states and shifts the pinning levels toward the band edges. These effects are assigned to adsorption and dissociation of water molecules, resulting in a passivation of intrinsic and extrinsic gap states. The results reveal a delicate interplay of intrinsic and extrinsic surface states at *m*-plane cleavage surfaces of GaN. The resulting doping dependence of the Fermi level pinning is a critical factor for the interpretation of tunneling spectra across doping profiles in group III-nitrides. Even more importantly, it demonstrates a strategy for achieving passivated flatband surfaces of nanowire-based optoelectronic, solar cell, and bio-electric devices as well as laser facets.

ACKNOWLEDGMENTS

The authors thank J. Friedrich and E. Würtz for the scanning electron microscopy measurements, U. Breuer for SIMS measurements, L. Lymperakis for scientific discussions, A. Redlich for literature research, and the Deutsche Forschungsgemeinschaft for financial support under Grant Nos. 398305088 and 390247238.

DATA AVAILABILITY

The data that support the findings of this study are available from the corresponding author upon reasonable request.

REFERENCES

[1]H. Morkoç, S. Strite, G. B. Gao, M. E. Lin, B. Sverdlov, and M. Burns, "Large-band-gap SiC, III-V nitride, and II-VI ZnSe-based semiconductor device technologies," J. Appl. Phys. **76**, 1363–1398 (1994).
[2]F. A. Ponce and D. P. Bour, "Nitride-based semiconductors for blue and green light-emitting devices," Nature **386**, 351–359 (1997).
[3]D. Zhu, D. J. Wallis, and C. J. Humphreys, "Prospects of III-nitride optoelectronics grown on Si," Rep. Prog. Phys. **76**, 106501 (2013).
[4]M. Kneissl, T.-Y. Seong, J. Han, and H. Amano, "The emergence and prospects of deep-ultraviolet light-emitting diode technologies," Nat. Photonics **13**, 1749–4893 (2019).
[5]B. Baur, G. Steinhoff, J. Hernando, O. Purrucker, M. Tanaka, B. Nickel, M. Stutzmann, and M. Eickhoff, "Chemical functionalization of GaN and AlN surfaces," Appl. Phys. Lett. **87**, 263901 (2005).
[6]W. Guo, M. Zhang, A. Banerjee, and P. Bhattacharya, "Catalyst-free InGaN/GaN nanowire light emitting diodes grown on (001) silicon by molecular beam epitaxy," Nano Lett. **10**, 3355–3359 (2010).
[7]Y.-J. Lu, C.-Y. Wang, J. Kim, H.-Y. Chen, M.-Y. Lu, Y.-C. Chen, W.-H. Chang, L.-J. Chen, M. I. Stockman, C.-K. Shih, and S. Gwo, "All-color plasmonic nanolasers with ultralow thresholds: Autotuning mechanism for single-mode lasing," Nano Lett. **14**, 4381–4388 (2014).
[8]S. Albert, A. Bengoechea-Encabo, X. Kong, M. A. Sanchez-Garcia, E. Calleja, and A. Trampert, "Monolithic integration of InGaN segments emitting in the blue, green, and red spectral range in single ordered nanocolumns," Appl. Phys. Lett. **102**, 181103 (2013).
[9]L. Lymperakis, P. H. Weidlich, H. Eisele, M. Schnedler, J.-P. Nys, B. Grandidier, D. Stievenard, R. E. Dunin-Borkowski, J. Neugebauer, and Ph. Ebert, "Hidden surface states at non-polar GaN ($10\bar{1}0$) facets: Intrinsic pinning of nanowires," Appl. Phys. Lett. **103**, 152101 (2013).
[10]V. Portz, M. Schnedler, H. Eisele, R. E. Dunin-Borkowski, and Ph. Ebert, "Electron affinity and surface states of GaN *m*-plane facets: Implication for electronic self-passivation," Phys. Rev. B **97**, 115433 (2018).
[11]Y. Wang, M. Schnedler, Q. Lan, F. Zheng, L. Freter, U. Breuer, H. Eisele, J.-F. Carlin, R. Butté, N. Grandjean, R. E. Dunin-Borkowski, and Ph. Ebert, "Interplay of anomalous strain relaxation and minimization of polarization changes at nitride semiconductor heterointerfaces," Phys. Rev. B (to be published) (2020).
[12]M. Schnedler, V. Portz, H. Eisele, R. E. Dunin-Borkowski, and Ph. Ebert, "Polarity-dependent pinning of a surface state," Phys. Rev. B **91**, 205309 (2015).
[13]M. Himmerlich, A. Eisenhardt, S. Shokhovets, S. Krischok, J. Räthel, Ph. Speiser, M. D. Neumann, A. Navarro-Quezada, and N. Esser, "Confirmation of intrinsic electron gap states at nonpolar GaN($1\bar{1}00$) surfaces combining photoelectron and surface optical spectroscopy," Appl. Phys. Lett. **104**, 171602 (2014).
[14]C. G. Van de Walle and D. Segev, "Microscopic origins of surface states on nitride surfaces," J. Appl. Phys. **101**, 081704 (2007).
[15]M. Landmann, E. Rauls, W. G. Schmidt, M. D. Neumann, E. Speiser, and N. Esser, "GaN *m*-plane: Atomic structure, surface bands, and optical response," Phys. Rev. B **91**, 035302 (2015).
[16]Ph. Ebert, L. Ivanova, and H. Eisele, "Scanning tunneling microscopy on unpinned GaN($1\bar{1}00$) surfaces: Invisibility of valence-band states," Phys. Rev. B **80**, 085316 (2009).
[17]J. G. Simmons, "Generalized formula for the electric tunnel effect between similar electrodes separated by a thin insulating film," J. Appl. Phys. **34**, 1793–1803 (1963).
[18]R. M. Feenstra and J. A. Stroscio, "Tunneling spectroscopy of the GaAs(110) surface," J. Vac. Sci. Technol. B **5**, 923–929 (1987).
[19]P. Quadbeck, Ph. Ebert, K. Urban, J. Gebauer, and R. Krause-Rehberg, "Effect of dopant atoms on the roughness of III-V semiconductor cleavage surfaces," Appl. Phys. Lett. **76**, 300 (2000).
[20]A. Lenz, "Atomic structure of capped In(Ga)As and GaAs quantum dots for optoelectronic devices," Ph.D. thesis (Technische Universität Berlin, 2008).
[21]S. Gaan, R. Feenstra, Ph. Ebert, R. Dunin-Borkowski, J. Walker, and E. Towe, "Structure and electronic spectroscopy of steps on GaAs(110) surfaces," Surf. Sci. **606**, 28–33 (2012).
[22]L. T. Romano, C. G. V. de Walle, J. W. Ager III, W. Götz, and R. S. Kern, "Effect of si doping on strain, cracking, and microstructure in GaN thin films grown by metalorganic chemical vapor deposition," J. Appl. Phys. **87**, 7745–7752 (2000).
[23]Q. Yan, A. Janotti, M. Scheffler, and C. G. Van de Walle, "Role of nitrogen vacancies in the luminescence of mg-doped gan," Appl. Phys. Lett. **100**, 142110 (2012).
[24]S. Limpijumnong and C. G. Van de Walle, "Diffusivity of native defects in GaN," Phys. Rev. B **69**, 035207 (2004).
[25]A. Kyrtsos, M. Matsubara, and E. Bellotti, "Migration mechanisms and diffusion barriers of carbon and native point defects in GaN," Phys. Rev. B **93**, 245201 (2016).

[26]J. L. Lyons and C. G. V. de Walle, "Computationally predicted energies and properties of defects in GaN," npj Comput. Mater. **3**, 12 (2017).
[27]N. Jäger, M. Marso, M. Salmeron, E. R. Weber, K. Urban, and Ph. Ebert, "Physics of imaging $p-n$ junctions by scanning tunneling microscopy and spectroscopy," Phys. Rev. B **67**, 165307 (2003).
[28]R. M. Feenstra, A. Vaterlaus, E. T. Yu, P. D. Kirchner, C. L. Lin, J. M. Woodall, and G. D. Pettit, "Atomic scale analysis of semiconductor interfaces," in *Semiconductor Interfaces at the Sub-Nanometer Scale* (Springer, Dordrecht, 1993), pp. 127–137.
[29]A. R. Smith, S. Gwo, K. Sadra, Y. C. Shih, B. G. Streetman, and C. K. Shih, "Comparative study of cross-sectional scanning tunneling microscopy/spectroscopy on III–V hetero- and homostructures: Ultrahigh vacuum-cleaved versus sulfide passivated," J. Vac. Sci. Technol. B **12**, 2610–2615 (1994).
[30]S. D. Wolter, "Kinetic study of the oxidation of gallium nitride in dry air," J. Electrochem. Soc. **145**, 629 (1998).
[31]I. Rousseau, G. Callsen, G. Jacopin, J.-F. Carlin, R. Butté, and N. Grandjean, "Optical absorption and oxygen passivation of surface states in III-nitride photonic devices," J. Appl. Phys. **123**, 113103 (2018).
[32]V. M. Bermudez and J. P. Long, "Chemisorption of H_2O on GaN(0001)," Surf. Sci. **450**, 98–105 (2000).
[33]P. Lorenz, "Oberflächen- und Grenzflächeneigenschaften von polaren galliumnitrid-schichten," Ph.D. thesis (Technische Universität Ilmenau, Fakultät für Mathematik und Naturwissenschaften, 2011).
[34]N. Kharche, M. S. Hybertsen, and J. T. Muckerman, "Computational investigation of structural and electronic properties of aqueous interfaces of GaN, ZnO, and a GaN/ZnO alloy," Phys. Chem. Chem. Phys. **16**, 12057–12066 (2014).
[35]X. Shen, P. B. Allen, M. S. Hybertsen, and J. T. Muckerman, "Water adsorption on the GaN $(10\bar{1}0)$ nonpolar surface," J. Phys. Chem. C **113**, 3365–3368 (2009).
[36]J. Wang, L. S. Pedroza, A. Poissier, and M. V. Fernández-Serra, "Water dissociation at the GaN$(10\bar{1}0)$ surface: Structure, dynamics and surface acidity," J. Phys. Chem. C **116**, 14382–14389 (2012).
[37]S.-Y. Wu, L.-W. Lang, P.-Y. Cai, Y.-W. Chen, Y.-L. Lai, M.-W. Lin, Y.-J. Hsu, W.-I. Lee, J.-L. Kuo, M.-F. Luo, and C.-C. Kuo, "Microscopic evidence for the dissociation of water molecules on cleaved GaN$(1\bar{1}00)$," Phys. Chem. Chem. Phys. **20**, 1261–1266 (2018).
[38]A. C. Meng, J. Cheng, and M. Sprik, "Density functional theory calculation of the band alignment of $(10\bar{1}0)$ In_xGa_1-xN/Water interfaces," J. Phys. Chem. B **120**, 1928–1939 (2016).
[39]L. Lymperakis, J. Neugebauer, M. Himmerlich, S. Krischok, M. Rink, J. Kröger, and V. M. Polyakov, "Adsorption and desorption of hydrogen at nonpolar GaN$(1\bar{1}00)$ surfaces: Kinetics and impact on surface vibrational and electronic properties," Phys. Rev. B **95**, 195314 (2017).
[40]P. Lorenz, R. Gutt, T. Haensel, M. Himmerlich, J. A. Schaefer, and S. Krischok, "Interaction of GaN(0001)-2×2 surfaces with H_2O," Phys. Status Solidi C **7**, 169–172 (2010).
[41]X. Zhang and S. Ptasinska, "Electronic and chemical structure of the H_2O/GaN(0001) interface under ambient conditions," Sci. Rep. **6**, 24848 (2016).
[42]M. Ptasinska, J. Piechota, and S. Krukowski, "Adsorption of hydrogen at the GaN$(000\bar{1})$ surface: An ab initio study," J. Phys. Chem. C **119**, 11563–11569 (2015).
[43]L. Janicki, J. Misiewicz, G. Cywiński, M. Sawicka, C. Skierbiszewski, and R. Kudrawiec, "Surface potential barrier in m-plane GaN studied by contactless electroreflectance," Appl. Phys. Express **9**, 021002 (2016).
[44]H. Wang, H. Zhang, J. Liu, D. Xue, H. Liang, and X. Xia, "Hydroxyl group adsorption on GaN (0001) surface: First principles and XPS studies," J. Electron. Mater. **48**, 2430–2437 (2019).
[45]M. Sato, Y. Imazeki, T. Takeda, M. Kobayashi, S. Yamamoto, I. Matsuda, J. Yoshinobu, Y. Nakano, and M. Sugiyama, "Atomistic-level description of GaN/water interface by a combined spectroscopic and first-principles computational approach," J. Phys. Chem. C **124**, 12466–12475 (2020).
[46]D. Franke, A. Luisa da Rosa, M. Lorke, and T. Frauenheim, "Electronic and optical properties of functionalized GaN-$(10\bar{1}0)$ surfaces using hybrid-density functionals," Phys. Status Solidi B **256**, 1800455 (2019).